BRAZILIAN JOURNAL OF PETROLEUM AND GAS
Journal Homepage: www.portalabpg.org.br/bjpg
A publication of the ABPG
BRAZILIAN ASSOCIATION OF R&D IN PETROLEUM AND GAS

$La_yCu_{0.4}Fe_{0.6}O_3$ PEROVSKITE OXIDES: SYNTHESIS, CHARACTERIZATION AND CATALYTIC REACTIVITY IN THE FISCHER-TROPSCH SYNTHESIS

[a] Souza, J. R. [1]; [a] Melo, M. A. F.; [b] Melo, D. M. A.; [a] Rojas, L. O. A.; [bc] Silva, C. F.; [b] Oliveira, F. S.

[a] Programa de Pós-Graduação em Engenharia Química - Universidade Federal do Rio Grande do Norte
[b] Programa de Pós-Graduação em Ciência e Engenharia de Materiais - Universidade Federal do Rio Grande do Norte
[c] Centro de Tecnologia do Gás Natural e Energias Renováveis

ABSTRACT

The current natural gas production of 52 $Mm^3 d^{-1}$ and the large projects for its expansion has been setting new boundaries for the Brazilian industry of oil and gas. So far, one of the biggest challenges regards the logistics for gas transportation from offshore fields. Therefore, the transformation of natural gas into gasoline, diesel and/or olefins via Fischer-Tropsch synthesis would be an alternative to this matter. In this work, the production of hydrocarbons by Fischer-Tropsch synthesis in a slurry reactor was investigated and a perovskite-type catalyst ($La_yCu_{0,4}Fe_{0,6}O_3$) was used, where the lanthanum index "y" varies from 0 to 1 on a molar basis. The selection of the method to synthesize perovskite largely depends on its target application and desired properties. The synthesized perovskites were characterized by X-ray diffraction (XRD) and energy dispersive X-ray fluorescence (EDX). The reducibility of such oxides was studied by a temperature-programmed reduction (TPR) technique and the reactivity of the catalysts was evaluated in a slurry reactor. The selectivity toward hydrocarbons was better in materials with a lanthanum content ranging between 0.6 and 0.8 to produce hydrocarbons (C_1-C_6 and C_{17}-C_{26}) from syngas by the Fischer-Tropsch (FT) synthesis.

KEYWORDS

Fischer-Tropsch; perovskites; TPR; slurry reactor

[1] To whom all correspondence should be addressed.
Address: Programa de Pós-Graduação em Engenharia Química, Universidade Federal do Rio Grande do Norte, Campus Universitário, Natal (RN), Brazil
CEP: 59072-970 | Telephone/Fax number: (55) 84 3215-3756 |e-mail: jrobert9@gmail.com
doi:10.5419/bjpg2011-0001

1. INTRODUCTION

Metal oxides and perovskite have been being employed as catalysts for various applications **(Tejuca and Fierro, 1993)**. $LaFeO_3$ and $CuFeO_3$ are important materials widely reported for various applications including solid oxide fuel cells **(Peña and Fierro, 1981)**, sensors **(Arai et al., 1986)**, oxygen permeation membranes **(Rodrigues et al., 2002)**, and as environmental catalysts **(Provendier et al., 1998)**. Conventionally, a solid-state oxide reaction method has been used to prepare $LaFeO_3$. This involves mechanical mixing of lanthanum oxide and iron oxide with subsequent calcination at temperatures higher than 1500 ^{o}C for nearly 48 h. This conventional route is employed due to simplicity and low manufacturing costs. The method results in a single perovskite phase. However, it is associated with drawbacks such as diffusional constraint, resulting in slow kinetics and high reaction temperatures, which promote uncontrolled particle size and lower surface area. Alternative routes to the solid-state reaction method are wet chemical synthesis methods such as co-precipitation, combustion, sol-gel and modified sol-gel methods **(Biniwale and Gosavi, 2010)**. In all these alternative methods, pure phase formation can be accelerated, as it involves mixing of elements at atomic level and lower calcination temperatures. In addition to this, it is possible to control particle size, morphology, surface area and pore size distribution. Various reports are available on $LaFeO_3$ and La_2CuO_4 perovskites due to their possible applications in various areas. Based on the target applications, different synthesis methods have been used by different researchers **(Li et al., 2001)**. In all these methods, the final calcinations temperatures were in the range of 500 – 950 °C.

A small number of copper compounds are known in which copper structurally occurs as Cu_3C **(Peña and Fierro, 1981; Tejuca and Fierro, 1993)**. Among these, the perovskite-type framework of $LaCuO_3$ enables the tuning of the nominal copper valence continuously from Cu_2C to Cu_3C. At ambient pressure La_2CuO_4 is a binary oxide mixture (La_2O_3–CuO). $LaCuO_3$ occurs only under high oxygen pressures **(Rodrigues et al., 2002)**. The high pressure synthesis of rhombohedral $LaCuO_3$ is achieved at 6.5 GPa and 1397 °C **(Tejuca and Fierro, 1993)**. $LaCuO_3$ can decompose to La_2CuO_4 and CuO or Cu_2O around 797 °C. It is a well-known fact that the catalytic properties of transition metal-containing perovskite-type oxides are strongly influenced by the oxidation state of the metal.

In this work $CuFeO_3$ doped with lanthanum at the *A* site of the ABO_3-type perovskite was synthesized by polymeric precursors, following the modified Pechini Method, and used as catalyst precursors in the Fischer-Tropsch reaction, using a gas feed of H_2/CO = 0.67 without dilution gas, with the purpose of simulating desirable industrial conditions. The effect of adding lanthanum to affect the catalytic activity and stability was examined. In order to characterize the different crystallographic phases prepared in this work, the Rietveld Method was used.

2. MATERIALS AND METHODS

2.1 Catalyst preparation

The preparation method of the $La_yCu_{0.4}Fe_{0.6}O_3$ perovskites (with "y" varying from 0 to 1 on a molar basis) consists in the polymerization of metallic chelates (polydented metallic complexes). In our case the citric acid (chelate agent) reacts with the metal sources (metallic salts) to form the polymetallic chelate. The poly-etherification reaction of the polymetallic chelate with ethylene glycol (Merck) and the simultaneous removal of the water formed lead to the formation of a polymeric resin. Then Fe-, Cu- and La-containing Merck nitrates were dissolved with citric acid, followed by the addition of ethylene glycol. The reaction occurred at about 90 °C and the water formed was evaporated until a vitreous resin was obtained. Next the gel was heated up to around 250 °C, a condition at which the ignition reaction occurs, producing a powdered precursor which still contains some carbon residue. In this case the resin was calcined under a static oxidant atmosphere from room temperature to 900 °C for 4 h at a heating rate of 10 °C min^{-1}. The copper and iron cations were placed in the *B* sites and the composition was fixed at 0.4 and 0.6 respectively. The lanthanum occupies the *A* sites, and its content varied between 0 and 1.

2.2 Catalyst characterization

The chemical composition of the catalyst was determined by energy dispersive X-ray fluorescence (EDX), in a Shimadzu EDX-700 equipment. X-ray diffraction (XRD) data were collected at room temperature in a Shimadzu XRD-6000 diffractometer equipped with a Cu-Kα source. Patterns were recorded between 5° and 80° (2θ scale) at a rate of 2° min^{-1}. For all cases, the crystallinity phases were identified with reference to powder diffraction data with the use of standard spectra software. The phase composition has been estimated by means of the Rietveld's powder structure refinement analysis (RF) of the XRD data.

Temperature Programmed Reduction (TPR) runs were carried out in a Micromeritics Autochem II 2920 equipment using about 30 mg of catalyst. The reactor was submitted to a linear temperature ramp from 25 to 900 °C at a heating rate of 10 °C min^{-1}, with a 10 % H_2/Ar gas flow at 50 standard cubic centimeter per minute (sccm) for 2 h. These experiments provide information on the reducibility of the catalysts, as evidenced by the reduction on the hydrogen peak. The catalytic evaluations were performed in a slurry-bed reactor, at CTGAS-ER facilities (Gas Technology and Renewal Energy Center, Brazil).

2.3 Catalytic tests

Catalytic tests under CO/H_2 were performed in a slurry reactor operating at 20 bar. An approximate mass of 2 g of catalyst was weighed and placed in the reactor. In order to disperse the catalyst and improve the heat and mass transfer, 40 mL of squalene were introduced as an inert starting fluid. After closing the reactor, it was heated up to 280 °C (10 °C min^{-1}) under a reducing flow (53.4 mL min^{-1} of H_2 and 79.6 mL min^{-1} of CO, with total flow of 133 mL min^{-1}), with a gas hourly space velocity (GHSV) of 4 and a H_2/CO molar ratio equal to 0.67. The reduction was carried out until the CO_2 concentration was stabilized. The pressure was then increased to 20 bar at a rate of 6 bar h^{-1} and the target temperature of 340 °C was reached at a rate of 10 °C min^{-1}.

The liquid products were collected through a hot trap (130 °C) and a cold trap (–2 °C). The outlet gases were analyzed with an online gas chromatograph (ThermoElectron Trace GC Ultra). CO conversion was calculated by mass balance at the entrance and exit of the reactor.

3. RESULTS AND DISCUSSION

3.1 Catalyst characterization

3.1.1 Chemical Composition

Table 1 shows the chemical composition of the synthesized materials by means of EDX. In all structures, the stoichiometric coefficients for lanthanum are very close, between 0.33 and 0.35. The same trend was observed for the other components, ranging from 0.33 to 0.36 for copper, and 0.31 to 0.32 for iron. Although the global compositions of the catalysts were almost the same, the difference in catalytic properties can be attributed to the composition of the phases present as oxides and perovskite, as discussed in the next section.

3.1.2 X-Ray Diffraction (XRD)

Although the XRD data of the materials show the presence of some phases other than the perovskite phase, they will be referred to by the general structure formula $La_yCu_{0.4}Fe_{0.6}O_3$. Other phases such as copper oxide, iron oxide and iron-copper oxide, rather than the perovskite phase, are encountered (Figure 4). There is also a material where no perosvkite phase is detected, a result that has not been reported frequently in the literature. This behavior is justified since the metal substitution is usually performed on the *B* site, and not on the *A* site.

Table 1. Theoretical and experimental (EDX) perovskite compositions.

y	Chemical composition	Experimental
0	$Cu_{0.4}Fe_{0.6}O_3$	$Cu_{0.49}Fe_{0.51}O_3$
0.2	$La_{0.2}Cu_{0.4}Fe_{0.6}O_3$	$La_{0.35}Cu_{0.33}Fe_{0.32}O_3$
0.4	$La_{0.4}Cu_{0.4}Fe_{0.6}O_3$	$La_{0.33}Cu_{0.36}\ Fe_{0.31}O_3$
0.6	$La_{0.6}Cu_{0.4}Fe_{0.6}O_3$	$La_{0.35}Cu_{0.33}Fe_{0.32}O_3$
0.8	$La_{0.8}Cu_{0.4}Fe_{0.6}O_3$	$La_{0.34}Cu_{0.35}Fe_{0.31}O_3$
1.0	$LaCu_{0.4}Fe_{0.6}O_3$	$La_{0.35}Cu_{0.34}Fe_{0.32}O_3$

The XRD diffraction patterns of the samples are presented in Figure 1. The diffractograms for the given samples presented basically the same diffraction profile. The diffractograms for the $La_yCu_{0.4}Fe_{0.6}O_3$ powders were compared to the Powder Diffraction Files of the International Centre for Diffraction Data, organization founded as the Joint Committee on Powder Diffraction Standards (JCPDS), and the reference files known as the JCPD card numbers. From these standards the peaks were identified as perovskite, Fe_2O_3 (JCPD 73-0603) and CuO (JCPD 80-1268) phases. It can also be seen that in the La-containing samples the perovskite phase diminished as the La content decreased, except when y = 0.2. Also the large peak at about 35° that appears in all diffraction patterns from y = 0.2 and higher, ascribed to perovskite, disappears in the absence of lanthanum. This is due to the perovskite phase transformation to a layered-type perovskite (Ruddlesden Popper series).

In Table 2 the cell parameters and the crystal system are presented for all materials. The copper-iron perovskite presented a cubic crystal system, and an orthorhombic configuration was detected for all compounds in the La series (JCPDS 74-2203). The *a*, *b* and *c* cell parameters were the same for all series, regardless of the lanthanum content.

The average crystallite size of the samples were calculated by the Rietveld method **(Rietveld, 1968)** using a specialized software. The data for crystallite size are listed in Table 3, where it is shown that the crystallite size decreases as the lanthanum content increases along the series, except for y = 0.2. All samples presented high crystalinity. In an ideal perovskite structure ($A_xB_yO_3$), atoms at *A* position are surrounded by 12 oxygen atoms, and 6 oxygen atoms surround the metal *B* site. When a trivalent atom at the *A* position is to be substituted by a bivalent (or tetravalent) ion, a change in the oxidation state of the *B* atom is induced, thereby changing their catalytic properties. The *B* atom with this new oxidation state reacts with the oxygen of the frame creating oxygen defects or excess (removal or addition of oxygen from or to the frame). For instance, cobalt in the *B* position induces oxygen defects in the frame structure, but for manganese perovskites there occurs oxygen excess. Iron **(Wu et al., 1989)** and nickel **(Yu et al., 1992)** perovskites present intermediate behaviors.

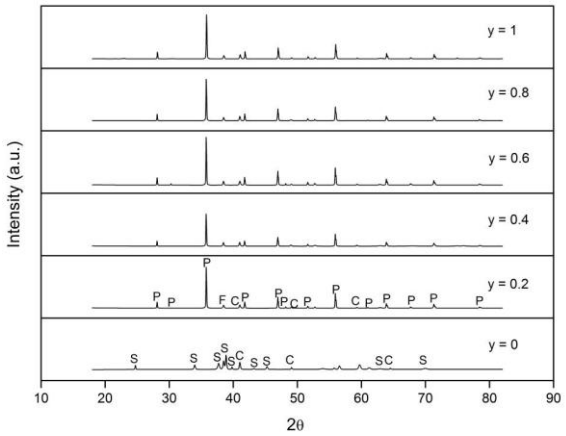

Figure 1. X-Ray diffraction patterns for $La_yCu_{0.4}Fe_{0.6}O_3$ perovskite; y = lanthanum content (% mol); P = perovskite; F = Fe_2O_3; C = CuO; S = perovskite RP.

The phases present in each sample were determined applying the Rietveld refinement method for the X-ray results. The phase distribution is presented in Table 4. This method confirmed the presence of secondary phases as noted previously by XRD. The $LaFeO_3$ phase percentage increases as the lanthanum content increases, except for y = 0.2.

In order to eliminate the secondary phases, the synthesis parameters must be optimized, which requires improved metal cation complexation during the formation of the citrates. Impurities detected in the precursor might have been carried along the synthesis procedures and might also be responsible for the perosvkite impurity.

Table 2. Lattice parameters and crystal system.

Sample	Crystal system	Lattice Parameters (Å)		
		a	b	c
$Cu_{0.4}Fe_{0.6}O_3$	Cubic	8.37	8.37	8.37
$La_{0.2}Cu_{0.4}Fe_{0.6}O_3$	Orthorhombic	5.55	5.56	7.87
$La_{0.4}Cu_{0.4}Fe_{0.6}O_3$	Orthorhombic	5.55	5.56	7.87
$La_{0.6}Cu_{0.4}Fe_{0.6}O_3$	Orthorhombic	5.55	5.56	7.87
$La_{0.8}Cu_{0.4}Fe_{0.6}O_3$	Orthorhombic	5.55	5.56	7.87
$LaCu_{0.4}Fe_{0.6}O_3$	Orthorhombic	5.55	5.56	7.87

Table 3. Crystallite size data for samples prepared using different lanthanum contents.

Sample	Crystallite size (nm)	Crystalinity (%)
$Cu_{0.4}Fe_{0.6}O_3$	121.06	80.62
$La_{0.2}Cu_{0.4}Fe_{0.6}O_3$	79.98	96.74
$La_{0.4}Cu_{0.4}Fe_{0.6}O_3$	97.05	79.80
$La_{0.6}Cu_{0.4}Fe_{0.6}O_3$	89.96	97.44
$La_{0.8}Cu_{0.4}Fe_{0.6}O_3$	90.30	93.08
$LaCu_{0.4}Fe_{0.6}O_3$	69.41	95.74

As shown in Figure 1 and Table 4, the catalysts show characteristic X-ray diffraction peaks of Fe_2O_3 that can be reduced to iron carbide **(Hong et al, 2001)**. The attribution of the formation of iron carbides is strongly related to the FT activity **(Li et al., 2001)**. Furthermore FeC, Fe_3O_4 and metallic iron have been proposed to be the active structures in the FT synthesis **(Hong et al., 2001)**. Thus, the catalytic activities could be explained by the extent of iron carbide formation **(Bian et al., 2002; Mansker et al., 1999)**.

3.1.3 TPR

Because the metal phase is the active phase in Fischer-Tropsch synthesis, attention was given to reducibility. The reduction was first followed by TPR. The hydrogen consumption profiles are presented in Figure 2 for the series of perovskites obtained.

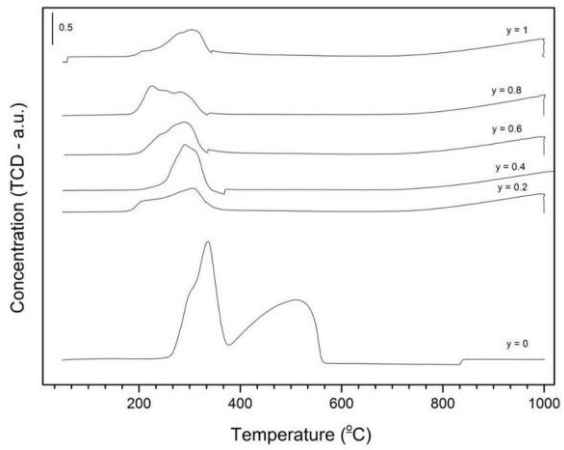

Figure 2. H_2 TPR profiles of $La_yCu_{0.4}Fe_{0.6}O_3$ (0 < y < 1)

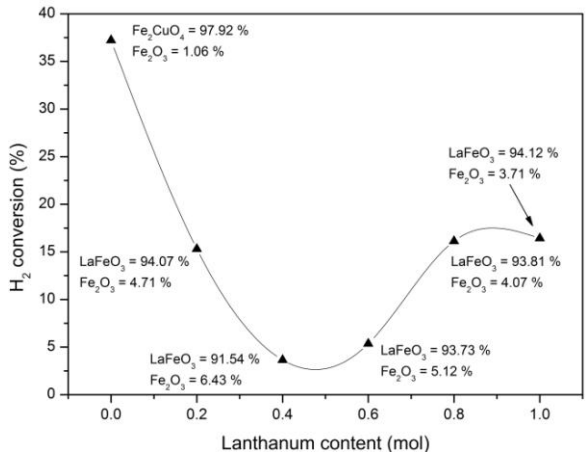

Figure 3. H_2 conversion as a function of the oxide phase.

Table 4. Phase identification by RF.

Sample	Phases (%)			
	$LaFeO_3$	Fe_2O_3	CuO	Fe_2CuO_4
$Cu_{0.4}Fe_{0.6}O_3$	-	1.06	1.02	97.92
$La_{0.2}Cu_{0.4}Fe_{0.6}O_3$	94.07	4.71	1.22	-
$La_{0.4}Cu_{0.4}Fe_{0.6}O_3$	91.54	6.43	2.03	-
$La_{0.6}Cu_{0.4}Fe_{0.6}O_3$	93.73	5.12	1.15	-
$La_{0.8}Cu_{0.4}Fe_{0.6}O_3$	93.81	4.07	2.12	-
$LaCu_{0.4}Fe_{0.6}O_3$	94.12	3.71	2.17	-

Table 5 presents the hydrogen uptake (expressed in volume, V) during the reduction events and the respective temperature reduction peaks. The reduction events were proposed after the deconvolution of the TPR spectra of Figure 2. The catalysts series present two main reduction events. For the first event, when one compares the hydrogen volume reacted in the copper-iron oxide with the lanthanum series, a remarkable reduction in the hydrogen uptake to less than half and a temperature shift (ΔT) of approximately –100 K are observed. For the lanthanum series small deviations in the hydrogen uptake and temperature reductions peaks were observed. These deviations cannot be correlated with the nominal lanthanum content. Jin and **Datye (2000)** noticed that simultaneous reduction of Fe_2O_3 and CuO occurs at an atomic ratio of Fe:Cu less than 60:40, and two distinct TPR peaks are observed at higher ratios due to their segregation. Under segregated conditions, the ability of Cu to dissociate hydrogen decreases, leading to a lower degree of reducibility of iron oxide, which eventually reduces the catalytic activity. The TPR results and the activity patterns of the present work also correlate well with these observations.

3.2 Catalytic Performance

3.2.1 Catalytic activity

The effect of hydrogen conversion over the $La_yCu_{0.4}Fe_{0.6}O_3$ series as a function of the lanthanum content is presented in Figure 3. The addition of lanthanum to the mixed oxide (Fe-Cu) leads to a decrease in conversion of about 50 %. For the lanthanum series the minimum hydrogen conversion is 3.6 % for y = 0.4, and a maximum of 16.5 % when y = 1.

Table 5. Peak reduction temperatures (T) and hydrogen uptakes (V) for the first (1) and second (2) reduction.

Sample	Reduction event	T / K	V / mL/g_{solid}	%
$Cu_{0.49}Fe_{0.51}O_3$	1. $Cu^{1+} == Cu^0$	568.05	73.845	20.709
	2. $Fe_3O_4 == FeO$	609.35	171.665	48.143
	3. $FeO == Fe^0$	784.48	111.064	31.148
$La_{0.35}Cu_{0.33}Fe_{0.32}O_3$	1. $Cu^{2+} == Cu^{1+}$	497.25	41.308	25.541
	2. $Fe_2O_3 == Fe_3O_4$	579.85	28.989	17.924
	3. Bulk Cu and Fe	1274.6	91.434	56.535
$La_{0.33}Cu_{0.36}Fe_{0.31}O_3$	1. $Cu^{1+} == Cu^0$ 2. $Fe_2O_3 == Fe_3O_4$	563.75	68.751	43.492
	3. Bulk Cu and Fe	1315	89.327	56.508
$La_{0.35}Cu_{0.33}Fe_{0.32}O_3$	1. $Cu^{2+} == Cu^{1+}$	525.75	27.093	19.093
	2. $Cu^{1+} == Cu^0$ 3. $Fe_2O_3 == Fe_3O_4$	561.95	31.570	22.247
	4. Bulk Cu and Fe	1265.5	83.240	58.660
$La_{0.34}Cu_{0.35}Fe_{0.31}O_3$	1. $Cu^{2+} == Cu^{1+}$	498.55	25.555	17.773
	2. $Cu^{1+} == Cu^0$ 3. $Fe_2O_3 == Fe_3O_4$	553.15	33.087	23.011
	4. Bulk Cu and Fe	1274.4	85.147	59.217
$La_{0.35}Cu_{0.34}Fe_{0.32}O_3$	1. $Cu^{1+} == Cu^*$	567.85	34.683	24.106
	2. $Fe_2O_3 == Fe_3O_4$	582.25	25.230	17.536
	3. Bulk Cu and Fe	1273.5	83.963	58.358

3.2.2 *Selectivity*

As mentioned above, Figure 3 presents the hydrogen conversion as a function the lanthanum content and the phase distribution. The mixed oxide (Fe_2CuO_4) conversion leads to 37 % conversion of hydrogen. When the lanthanum precursor is introduced during the synthesis a phase change occurs resulting in the appearance of the $LaFeO_3$ perovskite phase. For the $La_{0.4}Cu_{0.4}Fe_{0.6}O_3$ material (y = 0.4), this phase represents 92 % of the phase composition and its performance towards H_2 conversion was the worst of the series (3.67 %), which is about one tenth of the mixed oxide conversion. This material also exhibits the lowest crystallinity percentage.

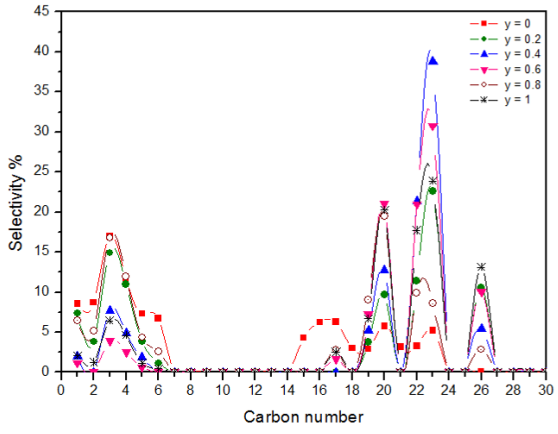

Figure 4. Product distribution.

As presented by **Voorhoeve et al. (1977)**, the CO oxidation occurs on the surface of the metal ion, therefore the catalytic activity of the CO oxidation depends strongly on the presence of the metal ion and the surface crystallinity. This relationship between H_2 conversion and crystallinity (except for $La_{0.6}Cu_{0.4}Fe_{0.6}O_3$, with y = 0.6) can be seen in Figure 3.

From the $LaFeO_3$ phase percentage shown in Figure 3, one can get a correlation between this phase and the H_2 conversion. It is clear that other features must be accounted for in order to optimize the catalyst, one of which is related to the product distribution, since selectivity is very important.

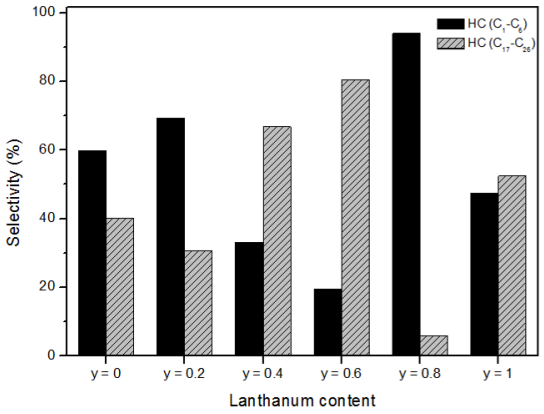

Figure 5. Hydrocarbon selectivity.

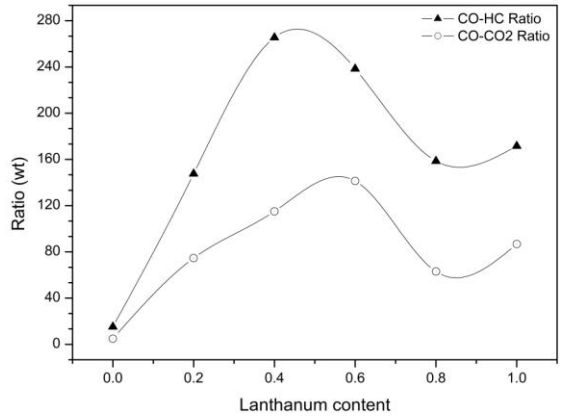

Figure 6. Mass of carbon monoxide formed per mass of hydrocarbon (CO/HC, ▲) or carbon dioxide (CO/CO_2, ○).

Although the conversion is not favored with the lanthanum addition (Figure 3), the selectivity for some hydrocarbons is increased, as shown in Figure 4, which depicts the product distribution as a function of the carbon number, and Figure 5, which refers to hydrocarbon selectivity as a function of the lanthanum content.

As shown in Figure 5, there is a trend for light hydrocarbon (C_1-C_6) selectivity, increasing from 60 % without lanthanum to 70 % when y = 0.2, finally reaching a maximum of 90 % when y = 0.8. For heavy cuts (C_{17}-C_{26}), there is an initial selectivity decrease from 40 % to 30 % due to the addition of lanthanum (y = 0.2) and then subsequent increments up to 65 % (y = 0.4), reaching a maximum of 80 % when y = 0.6, followed by a sharp decrease in selectivity to 5 % when y = 0.8. This type of plot is not expected for a Schultz-Flory distribution (SFD). It is known that this distribution

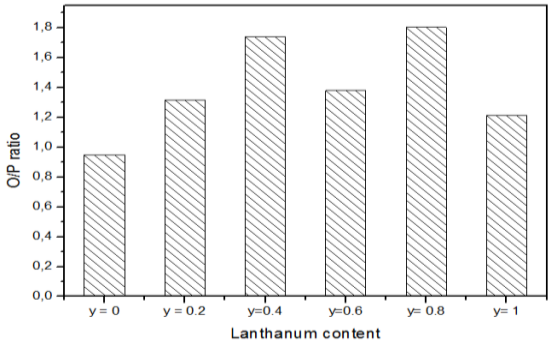

Figure 7. Olefin-to-paraffin ratio.

can be applied when there is equal probability of termination and chain propagation **(Steynberg and Dry, 2004)**, so this is not the case here. Primarily, one can distinguish between two main product distributions, typically for light and heavy cuts. For the selectivity of light cuts, the material with y = 0.8 is the best; on the other hand, the one with y = 0.6 is the most selective toward heavy cuts. Although not expected, this behavior is very interesting since it may be possible to tailor the selectivity toward light or heavy products according to the amount of lanthanum. This selectivity is more deeply discussed as follows.

The catalysts are also active to carbon dioxide formation (water-shift reaction), due to the presence of iron and copper. In order to compare between hydrocarbon (HC) and carbon dioxide formation, Figure 6 shows the ratios of CO:HC and $CO:CO_2$, presenting maxima with respect to the lanthanum load. For the hydrocarbon ratio this occurs at y = 0.4, and y = 0.6 for the $CO:CO_2$ ratio. These maxima represent the worst conversion-selectivity scenario towards the final product. In our case the hydrocarbons are the desired products and carbon dioxide is undesired. In general the production of carbon dioxide is favored when compared with hydrocarbons. Then, the best catalysts for hydrocarbon production are those with a lanthanum content of 0.2, although they are also more reactive to CO_2.

Finally, Figure 7 presents the olefin-to-paraffin (O/P) ratio in the products as a function of the lanthanum content. This ratio is very important to specify the product target. For olefin synthesis this ratio should be maximal. The O/P ratio is also higher for the lanthanum series compared with the lanthanum-free material – and actually doubles

when y = 0.8 (the best material). In all series, the O/P ratio is properly enhanced. As a general trend one can say that, in the lanthanum series, the O/P ratio increases with increasing lanthanum content.

4. CONCLUSIONS

Perovskites with high crystallinity were successfully prepared by polymeric precursors, following the modified Pechini Method. The perovskites obtained were influenced by the lanthanum added during the synthesis. The conversion and selectivity are very sensitive to the lanthanum content and the $LaFeO_3$ perovskite phase. The hydrogen conversion can be inversely correlated to the $LaFeO_3$ and directly to the crystallinity percentage. The formation of hydrocarbons is enhanced when lanthanum is incorporated in the $Cu_{0.4}Fe_{0.6}O_3$ oxide. The carbon product distribution for all the series suggests that the Schultz-Flory mechanism is not valid. This behavior enables to tailor the separation of hydrocarbons into light (C_1-C_6) and heavy (C_{17}-C_{26}) cuts. Similarly to the product distribution, the O/P ratio is dependent on the lanthanum content. The maximum O/P ratio (1.8) and selectivity to C_1-C_6 is obtained with the $La_{0.8}Cu_{0.4}Fe_{0.6}O_3$ material. The selectivity towards heavy hydrocarbons (C_{17}-C_{26}) is obtained with the $La_{0.6}Cu_{0.4}Fe_{0.6}O_3$ material. The carbon dioxide production is high, requiring a reduction on the water-shift reaction.

ACKNOWLEDGMENTS

The authors would like to acknowledge Center for Natural Gas Technologies and Renewal Energies (CTGAS-ER) for supporting this research.

5. REFERENCES

Arai, H.; Yamada, T.; Eguchi, K.; Seiyama, T. Catalytic combustion of methane over various perovskite-type oxides. **Applied Catalysis**, v. 26, p. 265-276, 1986. doi:10.1016/S0166-9834(00)82556-7

Bae, J. W.; Park, S.; Kang, S. H.; Lee, Yun-Jo; Jun, K. W. Effect of Cu content on the bifunctional Fischer-Tropsch Fe-Cu-K/ZSM5 catalyst**. Journal of Industrial and Engineering Chemistry,** v.15, p. 798-802, 2009. doi:10.1016/j.jiec.2009.09.002

Bian, G.; Oonuki, A.; Koizumi, N.; Nomoto, H.; Yamada, M.; Studies with a precipitated iron Fischer-Tropsch catalyst reduced by H_2 or CO. **Journal of Molecular Catalysis A**, v. 186, p. 203-213, 2002. doi:10.1016/S1381-1169(02)00186-3

Gosavi, P. V.; Biniwale, R. B. Pure phase $LaFeO_3$ perovskite with improved surface area synthesized using different routes and its characterization, **Materials Chemistry and Physics**, v. 119, p. 324-329, 2010. doi:10.1016/j.matchemphys.2009.09.005

Hong, J. S.; Hwang, J. S.; Jun, K. W.; Sur, J. C.; Lee, K. W. Deactivation study on a coprecipitated Fe-Cu-K-Al catalyst in CO_2 hydrogenation, **Applied Catalysis A: General**, v. 218, p. 53-59, 2001. doi:10.1016/S0926-860X(01)00617-2

Jin, Y.; Datye, A. K. Phase Transformations in Iron Fischer-Tropsch Catalysts during Temperature-Programmed Reduction. **Journal of Catalysis**, v. 196, p. 8-17, 2000. doi:10.1006/jcat.2000.3024

Li, S.; Li, A. Krishnamoorthy, S.; Iglesia, E. Effects of Zn, Cu, and K Promoters on the Structure and on the Reduction, Carburization, and Catalytic Behavior of Iron-Based Fischer–Tropsch Synthesis Catalysts. **Catalysis Letters**, v. 77, p.197-205, 2001. doi:10.1023/A:1013284217689

Mansker, L. D.; Jin, Y.; Bukur, D. B.; Datye, A. K. Characterization of slurry phase iron catalysts for Fischer-Tropsch synthesis. **Applied Catalysis A: General**, v. 186, p. 277-296, 1999. doi:10.1016/S0926-860X(99)00149-0

Peña, M.A.; Fierro, J.L.G. Chemical Structures and Performance of Perovskite Oxides. **Chemical Reviews**, v. 101, p. 1981-2018, 2001. doi:10.1021/cr980129f

Provendier, H.; Petit, C.; Roger, A. C.; Kiennemann, A. Influence of the precursors on the formation of a trimetallic defined structure. Application on Ni catalysts used for syngas obtention. In: Studies in Surface Science and Catalysis, Elsevier, 1998, v. 118, p. 285-294, Preparation of Catalysts VII, **Proceedings of the 7th International Symposium on Scientific Bases for the Preparation of Heterogeneous Catalysts**, Louvain-la-Neuve, Belgium, 1998. doi:10.1016/S0167-2991(98)80193-6

Rietveld H. M. A Profile Refinement Method for Nuclear and Magnetic Structures **Journal of Applied Crystallography**, v. 2 p. 65-71, 1969.

Steynberg, A.; Dry, M. **Fischer-Tropsch Technology** - Studies in Surface Science and Catalysis, The Netherlands, Elsevier, 2004.

Tejuca, L.G.; Fierro, J.L.G. **Properties and Applications of Perovskite Type Oxides**. New York: Dekker, 1993.

Voorhoeve, R. J. H.; Johnson, D. W., Jr.; Remeika, J. P.; Gallagher, P. K. Perovskite Oxides: Materials Science in Catalysis, **Science**, v. 195, p. 827-833, 1977. doi:10.1126/science.195.4281.827

Wu, Y.; Yu, T.; Dou, B. S.; Wang, C. X.; Xie, X. F.; Yu, Z. L.; Fan, S. R.; Fan, Z.R.; Wang, L. C. Comparative study on perovskite-type mixed oxide catalysts $A'_xA_{1-x}BO_{3-\lambda}$ (A' = Ca, Sr, A = La, B = Mn, Fe, Co) for NH_3 oxidation, **Journal of Catalysis**, v. 120, p. 88-107, 1989. doi:10.1016/0021-9517(89)90253-4

Yu, Z.; Gao, L.; Yuan, S.; Wu, Y. Solid defect structure and catalytic activity of perovskite-type catalysts $La_{1-x}Sr_xNiO_{3-\lambda}$ and $La_{1-1.333x}Th_xNiO_{3-\lambda}$, **Journal of the Chemical Society, Faraday Transactions**, v. 88, p. 3245-3249, 1992. doi:10.1039/ft9928803245